Dhaka Univ. J. Sci. 60(1): 87-91, 2012 (January)

STM Spectroscopy of Star-Type Molecular Magnet

M. S. Alam[1], F. A. Chowdhury[2], R. W. Saalfrank,[3] A. V. Postnikov,[4] and P. Müller[5]

[1]*Department of Physics, University of Dhaka, Dhaka-1000, Bangladesh*

[2]*Atomic Energy Centre, Dhaka, 4 Kazi Nazrul Islam Avenue, Dhaka-1000, Bangladesh*

[3]*Institut für Organische Chemie, Universität Erlangen-Nürnberg, Henkestr. 42, 91054 Erlangen, Germany*

[4]*Institut für Festkörperforschung, Forschungszentrum Jülich, 52452 Jülich, Germany*

[5]*Physikalisches Institut III, Universität Erlangen-Nürnberg, Erwin-Rommel-Str.1, 91058 Erlangen, Germany*

Email: alam@univdhaka.edu

Received on 09. 04. 2011. Accepted for Publication on 10.09.2011

Abstract

In order to achieve a better understanding of how scanning tunneling microscopy (STM) images of metallo-complexes are related to the geometric and electronic structure, we performed scanning microscopy (STM) and scanning tunneling spectroscopy (STS) techniques on $[Fe^{III}Fe^{III}_3\mathbf{L_6}]$ (L= N-methylaminediethanolate) star-type tetranuclear molecular magnet. The experiments were performed under ambient condition. We were able to image single molecule by STM with submolecular resolution. In our STS measurements we found a rather large signal at the positions of iron ion centers in the molecules. This direct addressing of metal centers was further confirmed by density functional theory (DFT) calculations.

I. Introduction

There is currently a great interest in the adsorption of large metallocomplexes or supramolecules on surfaces. Partly, this activity is due to the increasing use of large complexes for technological purpose. A new and promising approach to miniaturize the structures is the so-called "bottom-up" technique. The "bottom-up" technique is based on the formation of functional devices by special designed molecular building blocks. Recent progress in supramolecular coordination chemistry allows access to a broad variety of transition metal complexes. The ultimate limit of a functional device, e. g. a switch or transistor, can be considered as a single molecule. Consequently, with molecular electronics much smaller structures are feasible than with conventional semiconductor technology. For this current interest, large metal complexes or supramolecules are considered as potential building blocks for molecular electronics.[1] Progress and possibilities of metal complexes in molecular electronics has been reported recently, highlighting that the characteristics of metal complexes is attractive for the construction of highly integrated, functional molecular components.[2] Therefore, it is of high interest to investigate single magnetic molecules on surfaces which can be envisaged as memory elements for such type of electronics.

The scanning tunneling microscope (STM)[3] has been used to image a wide variety of adsorbate molecules on both metal and semiconductor surfaces. These molecules are insulating in their bulk structure.[4,5] Despite the lack of understanding of contrast mechanism, the STM was successfully used to image non-conducting materials at small bias voltages. [6, 7, 8] According to Tersoff and Hammans theory [9] for small voltage and constant tunneling current an STM image corresponds to map of constant local density of state at Fermi level. The energy gap between the HOMO and LUMO of isolated molecule is relatively large; therefore, the contribution to the density of states at the Fermi level is low. One might expect that organic molecules are not visible in the STM for low bias voltages. One possible explanation of this type of imaging could be as a result of broadening of HOMO and LUMO due to molecule-molecule or molecule-substrate interactions.[10]

Although the STM is capable of atomic resolution when imaging solid surfaces, mapping of large, complex molecules with submolecular resolution is a difficult task. An STM image contains both geometric and electronic information about the sample in a complicated way.[11] Even highly resolved STM topography images cannot provide information about specific features of large molecules. As, for example, if we would scan the van der Waals surface of large and complex molecules, we would see only a featureless ``blob`` of a large cluster of atoms. However, spectroscopic possibilities of STM allow us to probe electronic states of the molecules as a function of energy within a range of few eV around the Fermi level. [12, 13] If there would be subunits of the molecule exhibiting a special type of chemical bonding, STM spectroscopy allow filtering out special features of the species if they arise at energies well separated from the other states of the molecule.

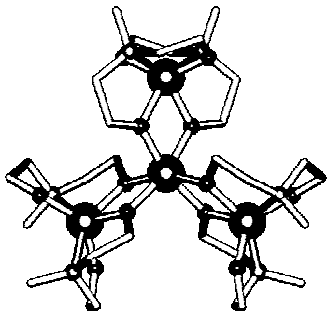

Fig.1. Schematic representation of the $[Fe^{III}Fe^{III}_3\mathbf{L_6}]$ complex ($\mathbf{L}$=$N(C_2H_5OH)_2CH_3$)[14].

The objective of this present work is to map topography as well as to study the specific features of the electronic properties at the single-molecule level. Scanning tunneling microscopy (STM) and scanning tunneling spectroscopy (STS) techniques were applied to one-dimensional chain, two-dimensional layers, and single molecules. The synthesis of the tetranuclear iron complex $[Fe^{III}Fe^{III}{}_3\mathbf{L_6}]$ **[**Figure1] has been reported earlier.[14] Recently the investigations of specific functionalities of molecular nanostructures under ambient conditions on surfaces were reviewed.[15,16] STS measurements are very often carried out under ultra high vacuum (UHV) conditions or UHV with low temperatures to increase signal-to-noise ratio. [17] However, it has been shown that under certain conditions STM experiments are also capable to detect local electronic properties at room temperature.[18] Using a home made STM working under ambient conditions, we succeeded to combine high resolution topography mapping with simultaneous current-voltage characteristics (STS) measurements on single molecules deposited on highly oriented pyrolytic graphite (HOPG) surface.

II. Experimental

The present STM investigations at the graphite-solution interface were performed with a home-built low drift STM head interfaced with a commercial controller and software (RHK Technology and ITHACO). Samples of $[Fe^{III}Fe^{III}{}_3\mathbf{L_6}]$ on HOPG surface were conveniently prepared by allowing 10^{-5} to 10^{-9} M CH_2Cl_2 solution to evaporate in air. Before adding the solution onto the substrate surface, we ensured that the tunneling tip had a sufficiently high resolution. We calibrated distances in the STM images by observing atomic spacing on HOPG. Typically, for the STM measurements, tunneling currents between 5 and 500 pA were employed. The bias voltage was ± 50 mV to ± 200 mV for topography measurements. The scan frequency was varied between 2 and 5 Hz. Resolution was 256×256 points for topography, and 128×128 in the CITS measurements. STM spectroscopy studies have been performed in the current imaging tunneling spectroscopy mode (CITS) simultaneously with constant current imaging using the interrupted-feedback-loop technique.[13] This was carried out by opening the feedback loop at a fixed separation between the tip and sample, and ramping of the bias voltage over the range of interest. The scan range of voltages was typically from -1 V to 0.1 V relative to the tip potential for approximately 100 discrete voltage steps. Typically, tunneling resistances of the order of 5 GΩ were set. We used Pt-Ir (90/10) tips mechanically cut from wires with a diameter of 0.25 mm.

III. Results and Discussion

After depositing the $[Fe^{III}Fe^{III}{}_3L_6]$ solution, we observed variety arrangements of molecules on HOPG surfaces. Step edge decoration by molecules or clusters of molecules has been observed which is usually ascribed to the Smoluchowski effect. [19] Figure 2 shows different moleculear arrangements, starting with single molecular lines or clusters of molecules (Figure 2a), regular arrangements of clusters of molecules (Figure 2b), a two-dimensional layer (Figure 2c), a single-molecular line (Figure 2d), dimeric combinations (Figure 2e), and even a single molecule (Figure 2f). Figure 2f displays an STM topography image of a $[Fe^{III}\ Fe^{III}{}_3\mathbf{L_6}]$ single molecule. In the background of Figure 2f underlying HOPG lattice are visible. In the STM image (Figure 2f), the apparent size of the single molecule is approximately 1.3 nm which is nicely conforming to the outer diameter of 1.2 nm calculated from X-ray data. The STM pictures could be reproducibly obtained with different samples and probes.

In order to study the electronic properties of $[Fe^{III}\ Fe^{III}{}_3\mathbf{L_6}]$ complex we applied current-imaging tunneling spectroscopy (CITS) technique. In current-imaging tunneling spectroscopy (CITS)[20] topography and current-voltage characteristics (I(V)) data are taken simultaneously. One then has a normal STM topography image, taken at constant tunneling current I, as well as current images, taken at constant-voltage (V).

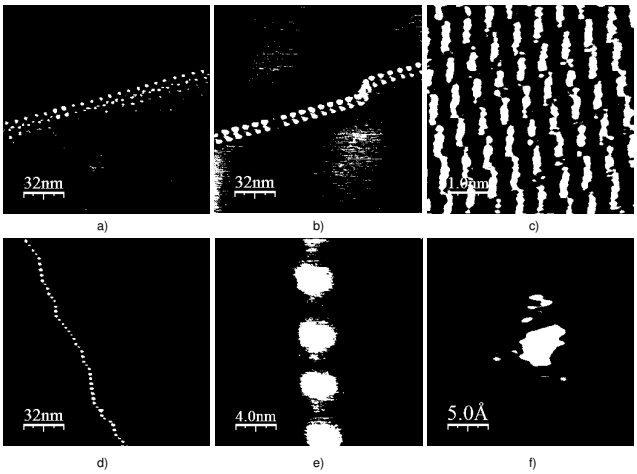

Fig. 2. STM results of $FeFe_3$ complexes deposited onto a HOPG surface.

Therefore, the current images are obtained from the three-dimensional data structure of I (V, x, y). The current image thus represents a slice, at a given voltage, of the current as a function of the lateral x, y coordinates. Variations on this scheme can be performed whereby I-V characteristics are recorded at a subset of points in a grid or along a particular line in an image. The current contrast changes significantly when at certain bias voltages new molecular energy levels come into play thus enhancing the information obtained from topography alone. The use of current imaging allows energy-resolved spectroscopy to be performed with spatial emphasis. One can see the location of the density of states of the molecule as a function of energy and position.[12]

CITS technique has been applied successfully to semiconductor materials but its application to organic molecules is rather difficult because of mobility or instability of the molecules, drift, etc. With our home built low drift STM head, we successfully applied this technique to the $[Fe^{III}Fe^{III}{}_3\mathbf{L_6}]$ star-type complex.

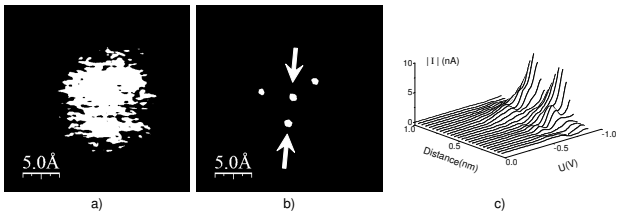

Fig. 3. Simultaneously recorded topography (a) and CITS current image (b) at bias voltage -938 mV of a $[Fe^{III}Fe^{III}_3\mathbf{L_6}]$ complex. (c) Representation of a set of I-V characteristics measured at 27 equidistant positions along a line between the two arrows in Figure 3b.

Figure 3 depicts a constant current topographic image (3a) and a CITS current image (3b) from a single scan. The topographic image presents a rather star like shape of the molecule with a diameter of approximately 1.3 nm which conforms to the outer diameter of the iron star. In contrast to this topography map, the CITS current map shows a sharp contrast at points which form a star pattern. Their distances nicely conform to the Fe-Fe ion distances as obtained from the X-ray structure of the molecule. This can be clearly seen in Figure 3c. Here, the full set of IV characteristics is plotted as |I| vs. Voltage and distance for the 27 positions between the arrows in Figure 3b. The background current arising from the HOPG surface has been subtracted. There are two ridges which are approximately 0.32 nm apart. This conforms to the distance between the center Fe ion and a peripheral Fe ion in the molecule.We note that there is a steep current increase at voltages below -0.75 V (Figure 3c). As all distances between the peaks conform to the Fe-Fe distances in the molecule, we conclude that we have mapped the local maxima of the density of states at the positions of the Fe ions. We did not get any significant signal arising from the ligands in our CITS measurements. This can be expected because their electronic states are far away from the Fermi level.[8] As a consequence, these states do not play a significant role in the tunneling current at bias voltages down to -1.0 V.

Figure 4a represents the color coded map of the DFT calculated charge density within an energy window between E_F and -0.95 eV in superposition with the crystal structure data (sticks). A 3D representation of the calculated electron density maps is shown in Figure 4b (upper row) using the same coloring scheme as the experimental data. Two energy windows are shown: The first one covers the range between E_F and the HOMO (-0.8 eV), while the second one covers range between E_F and all states within -1 eV. Bottom panel of Figure 4b shows the 3D energy-resolved spectroscopic maps taken at the applied voltages -0.78 V and -0.92 V with subtracted background. These voltages are corresponding to the two resonances observed in our measured spectra in Figure 3c. The comparison of our experimental results with theoretical calculations shows good agreement (Figure 4b).

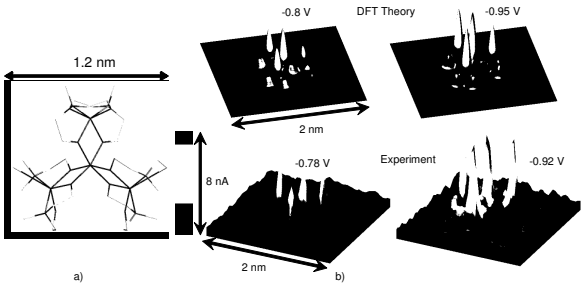

Fig. 4. Comparison of experimental CITS images of a single ferric star molecule on HOPG with theory.

The electronic structure of the $\{Fe^{III}[Fe^{III}(\mathbf{L}^1)_2]_3\}$ system in different magnetic configurations was calculated within the density functional theory (DFT), applying the calculation method and computer code SIESTA.[22] This method uses norm-conserving pseudopotentials and strictly localized basis functions of pseudoatomic orbitals. Calculations were performed for two settings: (a) an isolated molecule (118 atoms) put into a 22×22×18 Å simulation box, and (b) a true periodic crystal structure, as determined for a system crystallized with chloroform (see above), with the space group C2/c and 276 atoms per unit cell. The electronic properties discussed above are very close for both systems, therefore we present the figures related to a single-molecule case. Both sets of calculations used double-zeta basis according to classification, with polarization orbitals included for Fe and O. In the first-principles calculations of electronic structure, which were done in the framework of the density functional theory (DFT), we allowed a number of different orientations of Fe local moments. The comparison of corresponding total energies yielded an estimate of interatomic coupling parameters. A number of magnetic configurations, corresponding to different orientations of Fe local moments, have been considered; the comparison of the corresponding total energies yields an estimate of interatomic coupling parameters. A prerequisite for such a treatment is that each individual effective spin, associated with a Fe atom, maintains its identity (the value of local magnetic moment and its spatial localization) in the course of re-orientation. Indeed, the latter condition is well fulfilled, as in all studied spin arrangements we found the same value of local moment immediately localized at each Fe atom, 4 μ_B. This is accompanied, however, by an induced magnetization in the valence shells of neighbors, primarily oxygen ions, due to the 3*d*–O*p* hybridization. This increases the delocalized magnetic moment effectively associated with a Fe atom to 5 μ_B, which is consistent with the nominal

valence Fe^{III} and the expected individual spin 5/2 per Fe center.

Figure 5 shows local densities of states at the central and peripheral Fe atoms along with their next neighbors. One notes that the majority-spin states of Fe are fully occupied whereas minority-spin states are not quite empty, due to their interaction with oxygen 2*p* states; hence the local magnetic moment at the Fe sites is reduced from 5 to 4 μ_B (and the effective spin 5/2 is delocalized towards the oxygen neighbors). A separation of the Fe3*d* states into t_{2g}-like and e_g-like groups is very clear at the central site with its almost perfect octahedral surrounding, and is somehow smeared out at the peripheral site.

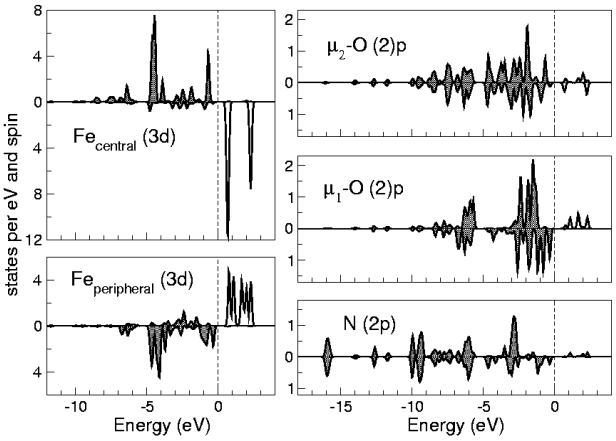

Fig. 5. Local densities of states of two Fe sites and their nearest neighbors. Occupied states are below zero energy.

Concerning the STM images discussed above, one can see from the DOS that at the applied voltage of up to 0.9 eV it is primarily the highest (e_g-like) peak of the occupied Fe DOS which contributes to the tunnel current. As the voltage decreases starting from zero, the peripheral Fe atoms yield the signal first followed by the central Fe atom – as it is indeed observed in STM experiments (here we did not present at low voltages current CITS maps). Simultaneously, there are noticeable O-related states within 0.9 eV below the Fermi level, which contribute to the complicated image shown in Figure 5 (upper row).

Figure 6 shows the spatial magnetization density in the ground-state magnetic configuration. One can well see that the spin density is concentrated at the Fe sites, but also around O and N of the ligands groups. The induced magnetization at the μ_2-oxygen atoms changes size at the nucleus, revealing the shape of 2*p* orbitals participating in the hybridization with Fe3*d*.

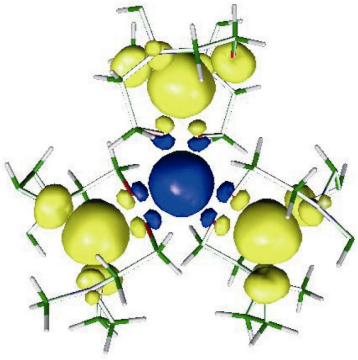

Fig. 6. Isosurfaces of the spin density at (± 0.01 e/ Å^3; "+" and "–" values are shown by the two colors) of the $\{Fe^{III}[Fe^{III}(L^1)_2]_3\}$ molecule in its ground state.

Whereas the ground-state configuration of the molecule is that with spin of the central Fe antiparallel to the three peripheral ones, in the calculation one can invert different spins in various combinations, which results in a sequence of metastable DFT solutions, with a certain hierarchy of total energies. The mapping of these results on the Heisenberg model, assuming first- and second-neighbors interactions as $H = -\sum_{i \neq j} J_{ij}\, \mathbf{S}_i\, \mathbf{S}_j$, yields $-J_{\text{central–peripheral}} = 10.8$ meV ≈ 126 K, and $-J_{\text{peripheral–peripheral}} = 0.3$ meV ≈ 3.5 K. This underlines the dominant role of interactions between nearest Fe neighbors and confirms their antiferromagnetic character. As for the interaction strength, one can note that similar estimations for the ferric wheels gave a Fe-Fe $-J$ parameter of about 80 K, whereas the fit of experimental data to the Heisenberg model yielded ≈ 20 K. Such overestimation by a factor ~4 is known to be due to insufficient inclusion of intra-atomic electron correlation effects in conventional DFT calculations. Consequently an error of the same order does probably occur for the present star-type system. We emphasize that the calculation predict a slight increase of interaction parameter as compared to the case of the ferric wheels.In our CITS measurements we observed only the metal centers of the $[Fe^{III}Fe^{III}_3\mathbf{L_6}]$ complex. Understanding the mechanism of this drastic enhancement is rather straightforward. Naturally, one would assume that the weakest bonds, i.e. the supramolecular coordination bonds, should dominate the molecular orbitals near the Fermi level of the molecule because this type of bonds has the lowest ionization energy. So ramping of the sample bias to negative values with respect to the tip, these levels are probed first. Therefore, beyond some threshold voltage, the STM current signal maps exclusively the electron concentration at the position of the metal ions even if these ions are covered by some parts of the ligands. A comparison of our measurements with

the DFT calculations shows clearly that this is indeed the case. Therefore, in this sense, STS spectroscopy directly addresses the metal centers in a rather complex molecule.

IV. Conclusion

The $[Fe^{III}Fe^{III}{}_3\mathbf{L_6}]$ star-type complex on HOPG substrates were imaged using an STM. Ordered lines of single molecules, dimeric combinations, regular molecule clusters, 2D monolayers, as well as individual molecules were observed with submolecular resolution. The size of the molecules observed is in good agreement as determined by X-ray crystallography. In STS measurements we were able to visualize the metal centers in the complex even they were completely covered by surrounding ligands. This direct addressing of the metal centers is consistent with DFT calculations. Such observations as this individual addressing of the metal centers inside a rather complex molecule highlight the dramatic advances that have been made in this area of nanotechnology, and a reason to hope that the future will allow the physics involved to have a practical place in future electronics components.

.....

1. Lehn, J. M., Supramolecular Chemistry-Concepts and Perspectives, VCH, Weinheim, 1995
2. Low, P. J., Dalton Trans., 2005, 2821.
3. Binnig, G.; H.Rohrer; C. Gerber; E. Weibel, Phys. Rev. Lett. 1982,**49**, 57.
4. Chiang, S.; H. J. Güntherodt; R. Wiesendanger, Scanning Tunneling Microscopy I, Springer-Verlag, Berlin, 1992, 182.
5. Jung, T. A.; F. J. Himpsel; R. R. Schlittler; J. K. Gimzewski; Wiesendanger, R. (Ed.), Scanning Probe Microscopy, Springer-Verlag, Berlin, 1998, 11.
6. Smith, D. P. E.; J., Vac. Sci. Technol., 1991, B 9, 1119.
7. Parks, D. C.; N. A. Clark; D. M. Walba; P. D. Beale, Phys. Rev. Lett., 1993, 70, 607.
8 Klusek, Z.; W. Kozlowski, J. Elect. Spect. and Relt. Phenom., 2000, 107, 6.
9. Tersoff, J.; D. R. Hamann, Phys. Rev., 1985, B 31, 805.
10. Fisher, A. J.; P. E. Blochl, Phys. Rev. Lett., 1993, 70, 3263.
11. Hembacher, S.; F. J. Giessibl, J. Mannhart, Phys. Rev. Lett., 2005, 94, 056101.
12. Scanning Tunneling Microscopy, Stroscio, J. A.; W. J. Kaiser; Eds. Academic Press, New York, 1993.
13. Alam, M. S.; V. Dremov; P. Müller; S. S. Mal; F. Hussain; U. Kortz, Inorg. Chem., 2006, 45, 2866.
14. Saalfrank, R. W.; I. Bernt; M. Chowdhry; F. Hampel; G. Vaughan, Chem. Eur. J., 2001, 7, 2765.
15. Feyter, D. S.; F. C. D. Schryver, Chem. Soc. Rev., 2003, 32, 139.
16. Samorí, P., Chem. Soc. Rev., 2005, 34, 55.
17. Wahl, P.; L. Diekhöner; M. Schneider; L. Vitali; G. Wittich; K. Kern, Phys. Rev. Lett. 93, 176603 (2004).
18. Miura, A.; Z. Chen; S. D. Feyter; M. Sdanowska; P. Jonkhejm; A. P. H. J. Schenning; B. Mejer; F. Würthner; F. C. D. Schryver, J. Am. Soc. Chem., 2003, 125, 14968.
19. Smoluchowski, R., Phys. Rev., 1941, 60, 661.
20. Novokmet, S.; M. S. Alam; V. Dremov; P. Müller; R. Alsfasser, Angew. Chem. Int. Ed. 2005, 44, 803.
21. Ordejón, P.; E. Artacho; J. M. Soler, Phys. Rev., 1996, B 53, R10441.
22. http://www.uam.es/siesta; (a) Ordejón P., E. Artacho and J. M. Soler, Phys. Rev. B 1996, 53, R10441; (b) Soler J. M., E. Artacho, J. D. Gale, A. García, J. Junquera, P. Ordejón and D. Sánchez-Portal, J.Phys.: Condens. Matter 2002, 14, 2745.